8-1-2010

III-nitride nanopyramid light emitting diodes grown by organometallic vapor phase epitaxy

Isaac Wildeson
Purdue Univ, Sch Elect & Comp Engn, iwildeson@purdue.edu

Robert Colby
Purdue University - Main Campus, rcolby@purdue.edu

David Ewoldt
Birck Nanotechnology Center, Purdue University, dewoldt@purdue.edu

Zhiwen Liang
Purdue University - Main Campus, liangz@purdue.edu

Dmitri Zakharov
Birck Nanotechnology Center, Purdue University, zakharov@purdue.edu

See next page for additional authors

Authors

Isaac Wildeson, Robert Colby, David Ewoldt, Zhiwen Liang, Dmitri Zakharov, Nestor J. Zaluzec, R. Edwin García, E A. Stach, and Timothy D. Sands

III-nitride nanopyramid light emitting diodes grown by organometallic vapor phase epitaxy

Isaac H. Wildeson,[1,3] Robert Colby,[2,3] David A. Ewoldt,[2,3] Zhiwen Liang,[2,3] Dmitri N. Zakharov,[3] Nestor J. Zaluzec,[4] R. Edwin García,[2,3] Eric A. Stach,[2,3] and Timothy D. Sands[1,2,3,a)]

[1]School of Electrical and Computer Engineering, Purdue University, West Lafayette, Indiana 47906, USA
[2]School of Materials Engineering, Purdue University, West Lafayette, Indiana 47906, USA
[3]Birck Nanotechnology Center, Purdue University, West Lafayette, Indiana 47906, USA
[4]Electron Microscopy Center, Materials Science Division, Argonne National Laboratory, Argonne, Illinois 60439, USA

Nanopyramid light emitting diodes (LEDs) have been synthesized by selective area organometallic vapor phase epitaxy. Self-organized porous anodic alumina is used to pattern the dielectric growth templates via reactive ion etching, eliminating the need for lithographic processes. (In,Ga)N quantum well growth occurs primarily on the six $\{1\bar{1}01\}$ semipolar facets of each of the nanopyramids, while coherent (In,Ga)N quantum dots with heights of up to ~ 20 nm are incorporated at the apex by controlling growth conditions. Transmission electron microscopy (TEM) indicates that the (In,Ga)N active regions of the nanopyramid heterostructures are completely dislocation-free. Temperature-dependent continuous-wave photoluminescence of nanopyramid heterostructures yields a peak emission wavelength of 617 nm and 605 nm at 300 K and 4 K, respectively. The peak emission energy varies with increasing temperature with a double S-shaped profile, which is attributed to either the presence of two types of InN-rich features within the nanopyramids or a contribution from the commonly observed yellow defect luminescence close to 300 K. TEM cross-sections reveal continuous planar defects in the (In,Ga)N quantum wells and GaN cladding layers grown at 650–780 °C, present in 38% of the nanopyramid heterostructures. Plan-view TEM of the planar defects confirms that these defects do not terminate within the nanopyramids. During the growth of p-GaN, the structure of the nanopyramid LEDs changed from pyramidal to a partially coalesced film as the thickness requirements for an undepleted p-GaN layer result in nanopyramid impingement. Continuous-wave electroluminescence of nanopyramid LEDs reveals a 45 nm redshift in comparison to a thin-film LED, suggesting higher InN incorporation in the nanopyramid LEDs. These results strongly encourage future investigations of III-nitride nanoheteroepitaxy as an approach for creating efficient long wavelength LEDs. © 2010 American Institute of Physics. [doi:10.1063/1.3466998]

I. INTRODUCTION

Nanoheteroepitaxy is an attractive approach towards achieving highly efficient light emitting diodes (LEDs). Specifically, one-dimensional nanostructures such as nanorods and nanowires offer the advantages of high light extraction efficiencies and the potential to be grown free of extended defects. The rejection of dislocations from nanorod and nanowire LEDs is particularly important for the III-nitride materials system for which threading dislocation densities of $10^8 - 10^{11}$ cm^{-2} are typical for thin-film heterostructures, depending on the growth conditions.[1] Various reports have demonstrated the growth of dislocation-free, one-dimensional III-nitride nanostructures.[2–6] Another inherent advantage of nanoheteroepitaxy is coherency strain relaxation. Theoretical investigations have demonstrated that lateral strain relaxation along the radial directions of nanorod and nanowire heterostructures allows a greater lattice mis-

match without the introduction of misfit dislocations as compared to a thin-film heterostructure.[7–9] Experimental observations also indicate that nanorods and nanowires have greater compliancy as compared to a thin film as the Young's modulus along the length of GaN nanowires was observed to decrease with diameters below 80 nm.[10] Reduced elastic modulus should allow greater InN incorporation in (In,Ga)N nanostructures—and thus a longer wavelength of emission—without the incorporation of misfit dislocations. The elimination of misfit dislocations in quantum wells with high InN content is necessary for creating highly efficient LEDs within the green/yellow portion of the visible spectrum where LED efficiencies are currently the lowest.[11]

Growth of GaN nanorods and nanowires has been realized by the use of rf-plasma-assisted molecular beam epitaxy (rf-MBE),[12] hydride vapor phase epitaxy (HVPE),[13] and organometallic vapor phase epitaxy (OMVPE).[3,14] Several groups have further processed one-dimensional LED nanostructures. The results have been very promising, leading to high internal quantum efficiencies (IQE) of 77% at 487 nm
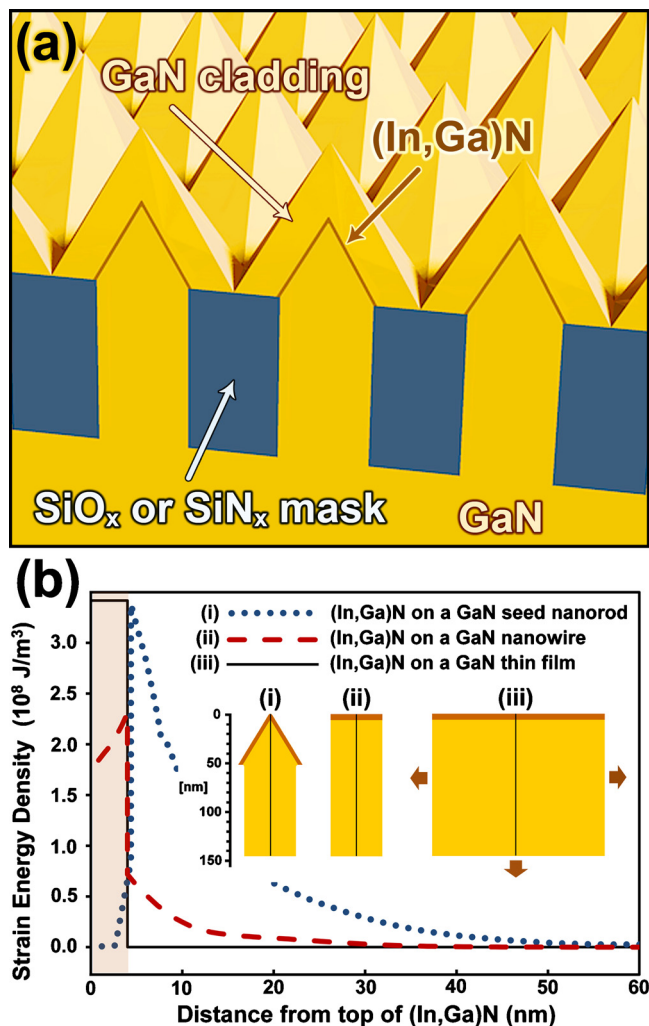
FIG. 1. (Color online) (a) Schematic of nanopyramid heterostructure design. (b) Strain energy density within an $In_{0.32}Ga_{0.68}N$ layer on (i) a pyramid-capped GaN seed nanorod of 142 nm height, (ii) a GaN nanowire of 142 nm height, and (iii) a semi-infinite GaN thin film. The width of both the GaN seed nanorod and GaN nanowire is 55 nm. The strain energy density profiles for the seed nanorod and the nanowire were simulated through 3D finite element analysis (Ref. 21), while that for the semi-infinite thin film was calculated analytically by assuming pseudomorphic $In_{0.32}Ga_{0.68}N$ growth (Ref. 22). The black lines in the cross-section schematics illustrate the length over which the strain energy density is plotted. The shaded region of the plot corresponds to the $In_{0.32}Ga_{0.68}N$ layer, and demonstrates that the strain energy density within the $In_{0.32}Ga_{0.68}N$ on the pyramid-capped GaN seed nanorod is the lowest.

in rf-MBE grown nanorods,[12] and high light extraction with 4.3 times the light output in metalorganic-HVPE grown nanorods, as compared to equivalent thin-film samples.[2] While these results demonstrate the strong potential of nanoheteroepitaxy within the III-nitride materials system, there are few reports of such LED nanostructures grown by OMVPE, the growth technique that is standard in the LED industry. Instead, a substantial portion of the OMVPE research has primarily focused on using nanorods and nanowires as growth templates for higher quality coalesced thin films.[15–17]

In this paper, a nonlithographic process for fabricating III-nitride nanopyramid LEDs by conventional OMVPE is presented [Fig. 1(a)]. The active region of these devices is located within a nanopyramid that grows atop a GaN seed nanorod. Controlled seed nanorod synthesis is achieved by selective area epitaxy through a dielectric template that also serves as a filter for the dislocations that thread through the underlying GaN film. This method allows direct control of diameter and position of seed nanorods. An additional benefit of this approach is that the hexagonal pyramid cap on each GaN seed nanorod is comprised of six semipolar $\{1\bar{1}01\}$ planes. (In,Ga)N quantum wells grown on $\{1\bar{1}01\}$ semipolar planes possess polarization-induced electric fields with magnitudes that are about a factor of ten lower than those in quantum wells of the same composition grown on c-plane GaN.[18] Previous work on LED heterostructures grown on planar semipolar GaN has resulted in the first true green laser from the III-nitrides, lasing at 531 nm,[19] and has demonstrated that the degree of efficiency droop is lower in LED structures grown on semipolar GaN as compared to those grown on polar c-plane GaN.[20] In addition, the pyramidal geometry on which the (In,Ga)N quantum wells are grown promotes significantly greater strain relaxation in the (In,Ga)N layer as compared to typical nanowire and thin-film heterostructures, as illustrated by the strain energy density plots in Figure 1(b). In the present study, porous anodic alumina (PAA) is used to pattern the dielectric growth template, eliminating the need for nanolithography. Specific investigations of structure, defect analysis and luminescent properties of the nanopyramids are reported below.

II. EXPERIMENTAL DETAILS

The starting substrates for this work were $5-8$ μm thick GaN films grown on c-plane sapphire by HVPE. Typical threading dislocation densities in the HVPE GaN films were $\sim 10^9$ cm^{-2}. The GaN surface was cleaned by a 5 min soak in 50 vol % HCl, followed by a 5 min rinse in deionized water. Following the cleaning treatment, 80–100 nm of electron-beam evaporated SiO_x or plasma enhanced chemical vapor deposited SiN_x was deposited on the GaN surface to serve as a dielectric growth template. While both SiO_x and SiN_x serve as effective templates for selective area epitaxy, SiN_x was used for electrically active devices in order to eliminate the possibility of oxygen doping within the p-GaN. The dielectric growth template was patterned using PAA as a reactive ion etch mask. Average pore diameters within the dielectric growth templates were ~ 55 nm. Details and parameters for the fabrication of the dielectric growth template can be found elsewhere.[14]

Selective area epitaxy of III-nitride nanopyramids was performed using an Aixtron 200HT OMVPE reactor. Prior to growth, samples were cleaned in piranha solution (3:1, sulfuric acid to hydrogen peroxide) for 3 min followed by a 3 min soak in deionized water. Growth of GaN seed nanorods was performed in the temperature range of $980°-1030$ °C with trimethylgallium and ammonia as the Ga and N sources, respectively. The flows of the trimethylgallium and ammonia were chosen for a low V/III molar ratio of 1430 so as to promote vertical growth.[1] Using hydrogen as a carrier gas, the seed nanorod growth time was 4.5 min at a total pressure of 100 torr. GaN seed nanorods were generally Si-doped under growth conditions that resulted in electron concentrations
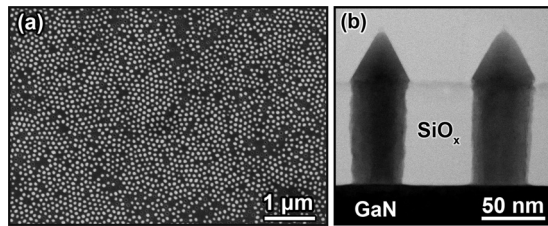
FIG. 2. (a) Plan-view FESEM of a GaN seed nanorod array selectively grown through a dielectric template. (b) Bright-field STEM cross-section of two typical GaN seed nanorods (grown at 1030 °C) with faceted pyramidal caps protruding above the dielectric template.
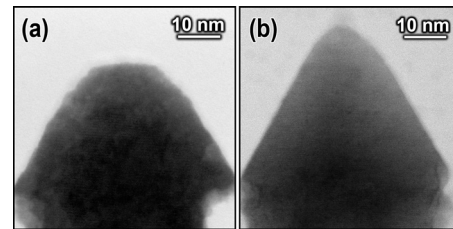

FIG. 3. Bright-field STEM images of GaN seed nanorods with (a) a truncated pyramidal cap grown at 980 °C and (b) a sharp pyramidal cap grown at 1030 °C.

of 2×10^{18} cm^{-3} for equivalent thin-film samples. Following the growth of the seed nanorods, the temperature was decreased to 650–780 °C for growth of an (In,Ga)N quantum well and a GaN cladding layer on the pyramidal caps of the seed nanorods. Typical parameters for (In,Ga)N quantum well growth were a V/III ratio of 7700, trimethylindium as the In source, and a total pressure of 100 torr. Typical parameters for the GaN cladding layer growth were 0.5 min of undoped GaN growth followed by 1.5 min of Mg-doped GaN growth, both performed with a V/III ratio of 1630, a growth temperature of 715 °C and a total pressure of 100 torr. Electrically active devices included additional Mg-doped p-GaN epitaxy at 1030 °C and subsequent magnesium activation steps that produced hole concentrations of 2×10^{17} cm^{-3} in thin films. Device isolation was achieved by chlorine-based inductively coupled plasma etching. Ohmic metal contacts were deposited by e-beam evaporation, using Ni/Au or Pt for p-GaN, and Ti/Al or In for n-GaN.

Characterization of the nanopyramid morphology was performed with a Hitachi S4800 field emission scanning electron microscope (FESEM), while analytical electron microscopy, transmission electron microscopy (TEM), and scanning transmission electron microscopy (STEM) studies were conducted using an FEI Titan 80-300 and an FEI Tecnai F20 operating at 300 kV and 200 kV, respectively. TEM was used to investigate the quality of the nanopyramid heterostructures, the associated lattice defects and local composition variation. Spectral imaging measurements were conducted using an ultrathin window EDAX-Sapphire Si(Li) energy dispersive spectrometer interfaced to a 4Pi-Revolution data acquisition system on the Tecnai F20. TEM samples were prepared by a focused ion beam (FIB) lift-out method with an FEI Nova 200 dual beam SEM/FIB equipped with a Klöcke nanomanipulator. In some instances, samples were further thinned using an argon ion mill at $\sim$1 kV (Gatan precision ion polishing system).

III. RESULTS AND DISCUSSION

A. GaN seed nanorods

Plan-view FESEM and cross-sectional TEM images show arrays of GaN seed nanorods with hexagonally faceted pyramidal caps selectively grown through dielectric templates (Fig. 2). The facets on the hexagonal pyramid are the six semipolar $\{1\bar{1}01\}$ planes. The seed nanorod growth self-terminates with the structure in Fig. 2 at the high growth

temperatures employed here. Epitaxial growth on the GaN seed nanorod structures must be reinitiated at lower growth temperatures, as will be discussed in detail in Sec. III B.

TEM examination further revealed that the seed nanorod morphology is dependent on growth temperature. Although seed nanorods grown at 1030 °C terminate with a pyramidal cap primarily comprised of six semipolar $\{1\bar{1}01\}$ facets (a "sharp" nanopyramid), seed nanorods grown at 980 °C also possess a basal facet at the apex of their cap (a "truncated" nanopyramid) (Fig. 3). As will be discussed in Sec. III B, the ability to alter the structure of the seed nanorod cap allows controlled variation in the heterostructures that can be grown subsequently. TEM examination also revealed that all GaN seed nanorods were free of dislocations that thread through the underlying HVPE GaN, affirming that the dielectric growth template serves as an efficient dislocation filter.[6,21]

B. Nanopyramid heterostructures

Nanopyramid heterostructure growth was performed on seed nanorods with both truncated and sharp caps. Nanopyramid heterostructures are comprised of the initial GaN seed nanorods, followed by (In,Ga)N quantum wells and GaN cladding layers. The resulting nanopyramid morphology is highly dependent on the growth temperature of the GaN cladding layers. Uniform cladding layers are essential for protecting the (In,Ga)N quantum well during the temperature ramp-up necessary for p-GaN growth and the undoped GaN serves as a diffusion barrier for the p-GaN dopant (magnesium), which has been shown to lower the IQE when diffused into the quantum well.[23] It was found that at low temperatures ($\sim$650 °C) selective area growth was no longer realized and polycrystalline GaN deposition was observed on the dielectric growth template. At higher temperatures of $\sim$780 °C, GaN cladding layer growth was nonuniform; many of the seed nanorods remained their initial size, while overgrowth on a few was substantial. Using the parameters employed in this work, growth at 715 °C resulted in the most uniform cladding layers.

The (In,Ga)N quantum well growth was initiated by outlining the profile of the GaN seed nanorods. However, by the end of the quantum well growth, the (In,Ga)N epitaxy resulted in a nanopyramid shell with a sharp apex. This was true for quantum well growth on seed nanorods with both sharp and truncated nanopyramid caps. In this fashion, the active region of the nanopyramid LED is either defined as quantum wells primarily located on the six semipolar $\{1\bar{1}01\}$
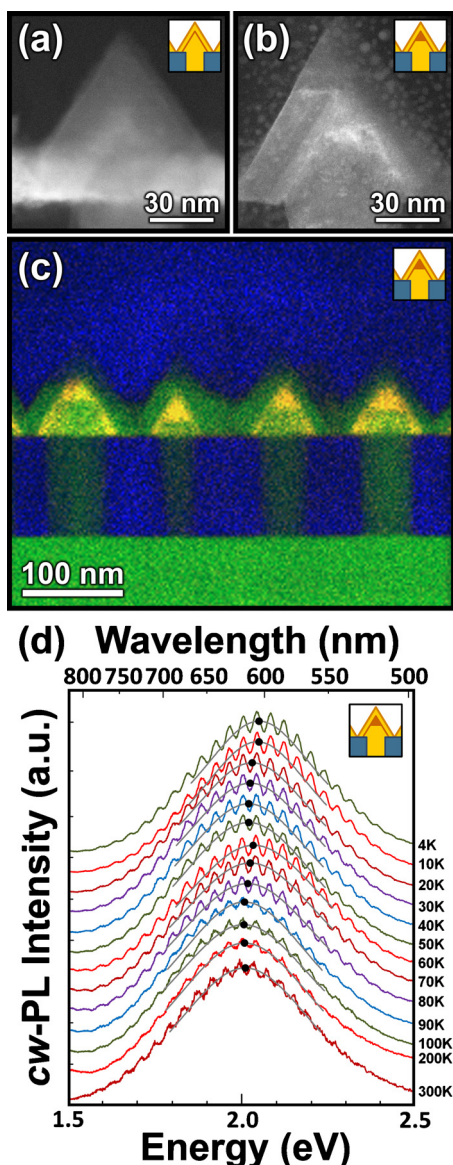
FIG. 4. (Color online) STEM cross-sections of nanopyramid heterostructures indicating the location of (In,Ga)N grown on both sharp (a) and truncated (b) seed nanorods. The truncated nanorod (b) was additionally thinned by Ar-ion milling, resulting in both the improved clarity over (a), and the resputtered copper particles (the bright dots). (c) X-ray spectral images of four complete nanopyramid heterostructures grown on truncated seed nanorods. The Ga–K signal is plotted in green, the In–L,K in red, and Si–K in blue, such that the yellow in the plot represents the combination of the Ga and In signals. (d) Temperature-dependent *cw*-PL of a heterostructure nanopyramid array grown on truncated seed nanorods using Voigt profiles (gray lines) for finding the peak energy of emission at each temperature. Data is normalized and shifted for clarity. Oscillations in the *cw*-PL intensity originate from the presence of a Fabry–Perot effect in the sapphire/GaN/air cavity.

facets by growing on seed nanorods with sharp nanopyramid caps, or as a quantum dot in addition to semipolar quantum wells by growing on seed nanorods with truncated nanopyramid caps [Figs. 4(a) and 4(b)]. The distribution of (In,Ga)N within complete nanopyramid heterostructures is shown by the partial "Z-contrast"[24] in the annular dark field (ADF) STEM images in Figs. 4(a) and 4(b). Here, heterostructure growth on seed nanorods with both truncated and sharp nanopyramid caps was investigated. The nanopyramid hetero-

structures grown on seed nanorods with truncated caps were additionally characterized with spectral imaging measurements, as shown in Fig. 4(c). Here, background subtracted integrated intensities were extracted for the Ga–K, the In–L and the In–K, and the Si–K x-ray emission lines, and the distribution of these three signals is mapped to red (In), green (Ga), and blue (Si) signals, which were overlayed into a 211×176 pixel elemental map. This overlay results in the (In,Ga)N layer appearing as a yellowish hue [Fig. 4(c)]. The background Si signal arises from the amorphous SiO_x present in the growth template and deposited atop the pyramids as a protective layer prior to TEM preparation. The spectral imaging results clearly indicate the outline of the truncated nanopyramid caps of the seed nanorods and demonstrate that the (In,Ga)N continued to grow to yield a sharp apex, in agreement with the ADF-STEM imaging. Also more evident in the spectral imaging is the presence of the solid, coherent (In,Ga)N hexagonal pyramid with a height of approximately 20 nm that forms a quantum dot within each nanopyramid grown on a truncated seed nanorod.

Nanopyramid heterostructures were characterized by temperature-dependent continuous-wave photoluminescence (*cw*-PL) with the use of a liquid helium cryostat. Prior to the *cw*-PL measurements, the dielectric growth masks were chemically removed by immersing the sample in buffered oxide etch. The excitation source was a 325 nm HeCd laser operating in the weak excitation regime, which has been recommended when using the ratio of integrated *cw*-PL intensity at 300 K to that at 4 K as an estimation of IQE.[25] Both excitation and collection were performed at approximately 45° from the surface normal of the sample. Figure 4(d) shows the *cw*-PL spectrum of the nanopyramid heterostructures at temperatures ranging from 300 to 4 K. Various oscillation peaks, spaced 38 meV apart, are observed in the *cw*-PL spectra due to the presence of a Fabry–Perot effect in the sapphire/GaN/air cavity, as was confirmed through the use of the analytical method described in Ref. 26 for a 7.2 μm GaN film (thickness confirmed by FESEM cross-section) and the 45° collection of the *cw*-PL.[27,28] Using Voigt profile fits for the emission spectra,[26] the peak wavelength of emission at each temperature was determined [Fig. 4(d)]. The peak wavelength of emission shifted from 617 nm at 300 K to 605 nm at 4 K, with full-width-at-half-maxima (FWHM) of 448 meV and 420 meV, respectively. The large FWHM may have resulted from the variation in size of the GaN seed nanorods on which the (In,Ga)N quantum wells were grown, as the standard deviation in pore diameter within the PAA-templated dielectric masks is about 10–15 nm.[14] Additionally, a spread in energy of emission is expected as the relaxed apices and faceted edges of the nanopyramids incorporate higher InN content during growth as compared to the $\{1\bar{1}01\}$ faces. Such results indicating inhomogeneity of InN incorporation during (In,Ga)N growth on pyramids have been experimentally reported by others.[29,30]

Using a Vegard approximation and the Varshni coefficients from Ref. 31, the anticipated redshift in emission from 4 to 300 K is 58 meV, which is larger than the 40 meV observed here.[32,33] However, typical temperature-dependent *cw*-PL of (In,Ga)N thin films and quantum wells demon-

strate peak emission energies that do not follow a Varshni profile with temperature, but instead an S-shape (redshift, blueshift, redshift) with increasing temperature. The S-shape dependence has been attributed to the involvement of band-tail states associated with composition fluctuations within the (In,Ga)N.[34,35] As demonstrated in Fig. 4(d), the position of peak emission energy from nanopyramid heterostructures followed a double S-shape (redshift, blueshift, redshift, blueshift) with increasing temperature. The peak emission energy initially redshifted 30 meV from 4 to 50 K, in comparison with an anticipated redshift from the Varshni expression for this change in temperature of only 2 meV. The peak emission energy then blueshifted 15 meV from 50 to 60 K. By considering the band-gap shrinkage of 1 meV caused by the temperature increase in this range, the actual blueshift was 16 meV. The turning temperature from redshift to blueshift observed here between 50 and 60 K is in close agreement with that reported in other studies of (In,Ga)N.[34,35] When the temperature was increased from 60 K to 100 K, the peak emission energy redshifted 29 meV, while the anticipated redshift was only 5 meV. As the temperature was increased above 100 K, the peak emission energy blueshifts 4 meV. By considering the band-gap shrinkage of 50 meV from 100 to 300 K, the estimated blueshift is 54 meV.

The double S-shape profile of peak emission energy with temperature has been previously observed in III-nitride films and was attributed to the contributions of two different groups of InN-rich features with different potential barriers.[36] Within the nanopyramid heterostructures, the two different groups of InN-rich features may arise from the enhanced InN incorporation at the relaxed apex of each of the nanopyramids and along the relaxed faceted edges that border the $\{1\bar{1}01\}$ planes of the nanopyramids, as these areas have demonstrated longer wavelengths of emission in (In,Ga)N grown on pyramids.[29,30] An alternative explanation for the second blueshift with increasing temperature is that the contribution from the commonly observed yellow defect luminescence in III-nitrides, typically observed at wavelengths lower than the (In,Ga)N emission demonstrated here, increases as the temperature approaches 300 K.[37,38] The wide FWHM of both the nanopyramid heterostructure emission and typical yellow defect luminescence prevents conclusive separation of the two possibilities from the recorded *cw*-PL data.

The integrated *cw*-PL intensity at 300 K was 10% of the integrated *cw*-PL intensity at 4 K. While the PL ratio is most likely an overestimate of the IQE—as the assumption that the IQE at 4 K is 100% has been shown to be false in some situations[39]—10% is among the highest reported PL ratios at wavelengths greater than 600 nm from the III-nitrides. An important caveat to these results is that further quantitative studies of the temperature dependence of the *cw*-PL signal is required in order to separate the contributions that may have arisen from yellow defect luminescence at 300 K, which is typically observed in PL or CL of GaN nanostructures.[40–42] In this work, nanopyramids grown without quantum wells did yield yellow luminescence with a peak wavelength of emission and an intensity that was weakly dependent on temperature (585 nm at 300 K and 588 nm at 4 K), as is typical
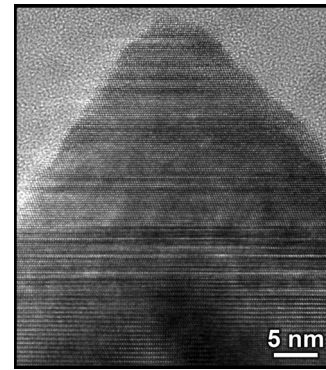

FIG. 5. Cross-sectional TEM image illustrating planar defects, both stacking faults and zincblende inclusions of thicknesses greater than 5 nm, within a GaN cladding layer grown at 715 °C from a nanopyramid heterostructure. 62% of nanopyramid heterostructures were free of extended defects, 38% contained clear planar faults, and 9% of the total included distinguishable zincblende inclusions.

for yellow defect luminescence in GaN.[37,38] Thus, for more accurate estimations of IQE by the PL ratio method, special care must be given to ensure that the contribution of yellow defect luminescence is not included in the integrated PL intensity at 300 K. Further clarification of IQE results can be achieved through the use of electroluminescent (EL) measurement techniques.[43,44]

C. Planar defects

Cross-sectional TEM investigation of GaN seed nanorods grown at 980–1030 °C revealed that these structures were free of dislocations and that the vast majority (>99.9% of the more than 3000 examined) were free of stacking faults, as in Fig. 2(b). However, planar defects were observed in some of the nanopyramid heterostructures grown at 650–780 °C. While 62% of nanopyramid heterostructures appeared free of extended defects, 38% contained clear planar faults, and 9% of the total included distinguishable zincblende inclusions in addition to stacking faults, often greater than 5 nm in thickness. Figure 5 illustrates one such nanopyramid heterostructure that includes both stacking faults and zincblende inclusions. Stacking faults and zincblende inclusions were apparent within the low temperature GaN cladding layer, even for samples that did not contain an (In,Ga)N quantum well. TEM cross-sectional imaging of the planar defects was performed for nanopyramid heterostructures grown on both sharp and truncated seed nanorods. The initiation point of the planar defects roughly corresponded to the apex of the underlying seed nanorod, with the average position of the planar defects on truncated seed nanorods being ~4 nm lower than for sharp seed nanorods. The percentages of nanopyramids containing planar defects were similar regardless of the shape of the seed nanorod. In both cases, the stacking faults were observed only at positions above the initial, high temperature seed nanorods. The zincblende inclusions, however, were only observed at positions above the apparent (In,Ga)N layer.

The presence of planar defects in GaN grown at low temperatures (650–780 °C) suggests that the adatom diffusivity in this temperature range is insufficient to guarantee
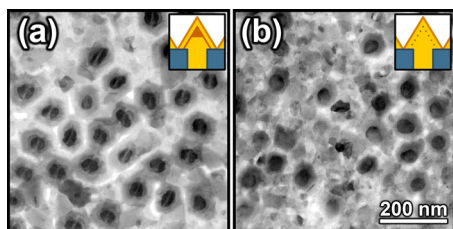
FIG. 6. (Color online) Plan-view bright-field STEM images of nanopyramid arrays obtained under similar imaging conditions (a) with (In,Ga)N quantum wells and (b) without (In,Ga)N quantum wells, illustrating the "coffee-bean"-like Ashby–Brown contrast arising from strain related to the (In,Ga)N quantum well. Images were acquired with a slight tilt for $\vec{g}\|\langle 11\bar{2}0\rangle$. The dashed line in the schematic of (b) illustrates the border between the high temperature GaN and the low temperature GaN.

that adatoms are binding in the most thermodynamically stable configurations. Planar defects through the (In,Ga)N quantum well and GaN cladding layer may have no significant effect on the performance of the nanopyramid LEDs, as the band offsets between the wurtzite and zincblende phase of the III-nitrides are modest.[45,46] However, the discontinuities in polarization arising at the wurtzite/zincblende phase interface may introduce electric fields in the cladding layer, as well as alter the magnitude of the electric fields in the quantum well.[45]

TEM analysis of thin-film samples grown in parallel with the investigated nanopyramid heterostructures revealed that these samples were free of planar defects. Thin-film samples are most likely resistant to the formation of low temperature growth mistakes due to the locally vicinal nature of their growth surface, which contains numerous atomic steps and ledges.[47] The steps and ledges provide favorable low energy sites for absorbing adatoms, and thus restrict a transition from the wurtzite AaBbAaBbAaBb stacking sequence to the zincblende AaBbCcAaBbCc stacking sequence. However, growth at the apex of a nanopyramid occurs on a small area that may well be free of steps and ledges. The result is a Frank–Van der Merwe, layer-by-layer growth mode that may increase the chance of incorporating a fault in the stacking sequence. In addition, by using selective area epitaxy for the synthesis of the nanopyamids, the majority of the surface is covered by a dielectric template on which neither Ga nor GaN can nucleate. This results in a significantly larger effective adatom flux onto the growth surface of the nanopyramids as compared to a thin-film surface, which additionally increases the chances of introducing planar defects.

All nanopyramid planar defects appeared continuous when viewed in cross-section; however, cross-sectional views are not well suited for identifying the dislocations that might be associated with planar defects in GaN. Plan-view TEM samples were investigated for nanopyramids with and without (In,Ga)N quantum wells, to confirm that the planar defects did not terminate within the nanopyramids and, thus, leave behind bound partial dislocations. The plan-view images revealed dislocation-free nanopyramids, indicating that the stacking faults and zincblende inclusions are continuous, sweeping completely through the nanopyramids (Fig. 6). The continuous nature of the planar defects is advantageous from
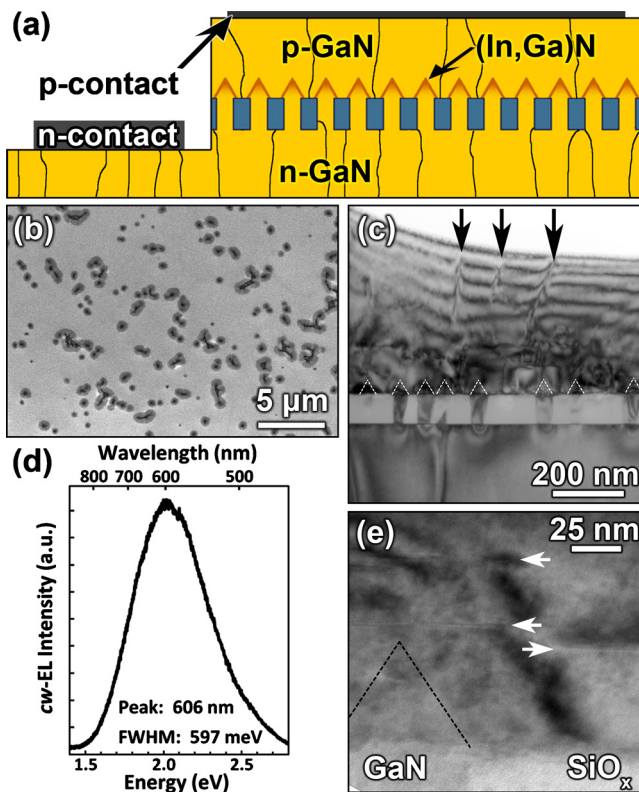

FIG. 7. (Color online) (a) Schematic of complete LED heterostructure. Black lines in schematic illustrate threading dislocations. (b) Plan-view FESEM after p-GaN growth that results in a partially coalesced film. (c) Bright-field TEM image illustrating three threading dislocations arising from merging nanopyramids. Some of the seed nanorods in this section are almost entirely milled away in the process of making a cross-section thin enough for TEM. Fringes in image result from small changes in the sample thickness. (d) Room temperature *cw*-EL spectrum collected from a nanopyramid LED grown on sharp seed nanorods. (e) Bright-field TEM cross-section illustrating the termination of three planar defects (termination points indicated by arrows) during the merging of nanopyramids. The dashed lines in (c) and (e) indicate the locations of (In,Ga)N active regions.

an LED device standpoint, as nonradiative defects are not introduced in close proximity to the quantum well. Ashby–Brown, or "coffee-bean," contrast was observed in the bright-field TEM and STEM images of nanopyramids containing (In,Ga)N quantum wells [Fig. 6(a)]. Ashby–Brown contrast indicates strain in a film induced by a lattice-mismatched inclusion.[48] In this study, the lattice-mismatched inclusion is the (In,Ga)N quantum dot near the apex of each nanopyramid. The Ashby–Brown contrast is not observed in nanopyramids that do not contain (In,Ga)N quantum wells.

D. Nanopyramid LEDs

Following the synthesis of nanopyramid heterostructures, p-type GaN growth was required to make complete, electrically active devices. P-type GaN growth was initiated during a 3 min temperature ramp-up from 715 to 1030 °C in order to provide greater uniformity in the coverage of the initial growth. An additional 27 min of p-type GaN epitaxy was performed at 1030 °C, resulting in a partially coalesced film covering the nanopyramid array, as illustrated by the plan-view FESEM in Fig. 7(b). The transition from pyramidal to thin-film geometry results from the relatively close

spacing of the seed nanorods and the thickness required to create an undepleted p-GaN layer. Figure 7(a) shows a schematic illustrating the resulting LED structure. New dislocations are introduced in the p-GaN when the initially pyramidal cladding layers coalesce into a film, often clearly associated with the termination of planar defects as nanopyramids merge [Fig. 7(e)]. Other threading dislocations may result from the misalignment of atomic planes as the nanopyramids relax with respect to the substrate. In the bright-field TEM cross-section in Fig. 7(c), three such threading dislocations are discernable. It is important to note that the newly introduced dislocations, either partial or threading, do not traverse the active region of the nanopyramids [Fig. 7(e)]. However, the specific role of these dislocations in the performance of the LED devices is still under investigation. If the spacing of the nanopyramids were increased so that a sufficient p-GaN thickness was achieved without nanopyramid impingement, the formation of new dislocations would be prevented.

Following growth, device structures were isolated via optical lithography and chlorine-based inductively coupled plasma etching, and metal contacts were deposited. Figure 7(d) shows *cw*-electroluminescence (*cw*-EL) results that were collected directly normal to a nanopyramid LED device grown on sharp seed nanorods. The peak wavelength of emission was at 606 nm, and similar to the *cw*-PL measurements of nanopyramid heterostructures, the *cw*-EL spectrum possesses a wide FWHM of emission (597 meV). A thin-film device grown in parallel with the nanopyramid LED yielded a peak wavelength of emission at 561 nm. The 45 nm (160 meV) redshift observed between the nanopyramid and thin-film LEDs may have resulted from higher InN incorporation on the relaxed nanopyramids. The degree of the observed redshift between the nanopyramid and thin-film LEDs agrees well with results reported by Zang *et al.*[49]

IV. SUMMARY

Nanopyramid heterostructures were selectively grown by OMVPE through a PAA-derived dielectric template and electrically active nanopyramid LEDs were fabricated. TEM analysis revealed that GaN seed nanorods were free of threading dislocations, while low temperature (In,Ga)N quantum well and GaN cladding layer growth resulted in continuous planar defects within some of the nanopyramids. Upon merging of nanopyramids, dislocations were introduced within the coalesced p-GaN film. While none of the dislocations intersected the active region of the devices, their exact role on the performance of the LEDs merits future investigation. Quantum wells were grown on semipolar $\{1\bar{1}01\}$ planes, and control of the (In,Ga)N quantum dot size has been demonstrated by altering the seed nanorod geometry. Temperature-dependent *cw*-PL investigations revealed a double S-shape dependence of peak emission energy with increasing temperature, and an integrated *cw*-PL ratio of 10% for 300 K:4 K. A longer peak wavelength of *cw*-EL is observed in nanopyramids as compared to thin-film LEDs, which suggests suppressed desorption of InN due to strain relaxation in nanopyramid heterostructures during quantum

well growth. These results encourage further investigations of nanoheteroepitaxy as an approach for creating efficient long wavelength, III-nitride LEDs.

[1] P. Gibart, Rep. Prog. Phys. **67**, 667 (2004).
[2] H. M. Kim, Y. H. Cho, H. Lee, S. I. Kim, S. R. Ryu, D. Y. Kim, T. W. Kang, and K. S. Chung, Nano Lett. **4**, 1059 (2004).
[3] S. D. Hersee, X. Sun, and X. Wang, Nano Lett. **6**, 1808 (2006).
[4] F. Qian, S. Gradecak, Y. Li, C. Y. Wen, and C. M. Lieber, Nano Lett. **5**, 2287 (2005).
[5] M. A. Mastro, J. A. Freitas, Jr., M. Twigg, R. T. Holm, C. R. Eddy, Jr., F. Kub, H. Y. Kim, J. Ahn, and J. Kim, Phys. Status Solidi A **205**, 378 (2008).
[6] R. Colby, Z. Liang, I. H. Wildeson, D. A. Ewoldt, T. D. Sands, E. A. Stach, and R. E. Garcia, Nano Lett. **10**, 1568 (2010).
[7] S. Luryi and E. Suhir, Appl. Phys. Lett. **49**, 140 (1986).
[8] D. Zubia and S. D. Hersee, J. Appl. Phys. **85**, 6492 (1999).
[9] E. Ertekin, P. A. Greaney, D. C. Chrzan, and T. D. Sands, J. Appl. Phys. **97**, 114325 (2005).
[10] C. Y. Nam, P. Jaroenapibal, D. Tham, D. E. Luzzi, S. Evoy, and J. E. Fischer, Nano Lett. **6**, 153 (2006).
[11] G. Chen, M. Craven, A. Kim, A. Munkholm, S. Watanabe, M. Camras, W. Götz, and F. Steranka, Phys. Status Solidi A **205**, 1086 (2008).
[12] H. Sekiguchi, K. Kishino, and A. Kikuchi, Appl. Phys. Express **1**, 124002 (2008).
[13] H. M. Kim, D. S. Kim, D. Y. Kim, T. W. Kang, Y. H. Cho, and K. S. Chung, Appl. Phys. Lett. **81**, 2193 (2002).
[14] P. Deb, H. Kim, V. Rawat, M. Oliver, S. Kim, M. Marshall, E. Stach, and T. Sands, Nano Lett. **5**, 1847 (2005).
[15] T. Y. Tang, W. Y. Shiao, C. H. Lin, K. C. Shen, J. J. Huang, S. Y. Ting, T. C. Liu, C. C. Yang, C. L. Yao, J. H. Yeh, T. C. Hsu, W. C. Chen, H. C. Hsu, and L. C. Chen, J. Appl. Phys. **105**, 023501 (2009).
[16] K. Y. Zang, Y. D. Wang, S. J. Chua, L. S. Wang, S. Tripathy, and C. V. Thompson, Appl. Phys. Lett. **88**, 141925 (2006).
[17] S. C. Ling, C. L. Chao, J. R. Chen, P. C. Liu, T. S. Ko, T. C. Lu, H. C. Kuo, S. C. Wang, S. J. Cheng, and J. D. Tsay, Appl. Phys. Lett. **94**, 251912 (2009).
[18] S. H. Park and D. Ahn, Appl. Phys. Lett. **90**, 013505 (2007).
[19] Y. Enya, Y. Yoshizumi, T. Kyono, K. Akita, M. Ueno, M. Adachi, T. Sumitomo, S. Tokuyama, T. Ikegami, K. Katayama, and T. Nakamura, Appl. Phys. Express **2**, 082101 (2009).
[20] H. Zhong, A. Tyagi, N. N. Fellows, F. Wu, R. B. Chung, M. Saito, K. Fujito, J. S. Speck, S. P. DenBaars, and S. Nakamura, Appl. Phys. Lett. **90**, 233504 (2007).
[21] Z. Liang, R. Colby, I. H. Wildeson, D. A. Ewoldt, T. D. Sands, E. A. Stach and R. E. García, J. Appl. Phys. (to be published).
[22] J. F. Nye, *Physical Properties of Crystals: Their Representation by Tensors and Matrices* (Oxford University Press, New York, 1985).
[23] K. Köhler, T. Stephan, A. Perona, J. Wiegert, M. Maier, M. Kunzer, and J. Wagner, J. Appl. Phys. **97**, 104914 (2005).
[24] S. J. Pennycook and D. E. Jesson, Phys. Rev. Lett. **64**, 938 (1990).
[25] S. F. Chichibu, A. Uedono, T. Onuma, B. A. Haskell, A. Chakraborty, T. Koyama, P. T. Fini, S. Keller, S. P. Denbaars, J. S. Speck, U. K. Mishra, S. Nakamura, S. Yamaguchi, S. Kamiyama, H. Amano, I. Akasaki, J. Han, and T. Sota, Nature Mater. **5**, 810 (2006).

[26]C. Hums, T. Finger, T. Hempel, J. Christen, A. Dadgar, A. Hoffmann, and A. Krost, J. Appl. Phys. **101**, 033113 (2007).

[27]A. Billeb, W. Grieshaber, D. Stocker, E. F. Schubert, and R. F. Karlicek, Jr., Appl. Phys. Lett. **70**, 2790 (1997).

[28]T. Kawashima, H. Yoshikawa, S. Adachi, S. Fuke, and K. Ohtsuka, J. Appl. Phys. **82**, 3528 (1997).

[29]V. Pérez-Solórzano, A. Gröning, M. Jetter, T. Riemann, and J. Christen, Appl. Phys. Lett. **87**, 163121 (2005).

[30]P. R. Edwards, R. W. Martin, I. M. Watson, C. Liu, R. A. Taylor, J. H. Rice, J. H. Na, J. W. Robinson, and J. D. Smith, Appl. Phys. Lett. **85**, 4281 (2004).

[31]I. Vurgaftman and J. R. Meyer, J. Appl. Phys. **94**, 3675 (2003).

[32]E. F. Schubert, *Light-Emitting Diodes*, 2nd ed. (Cambridge University Press, New York, 2006).

[33]Y. P. Varshni, Physica **34**, 149 (1967).

[34]Y. H. Cho, G. H. Gainer, A. J. Fischer, J. J. Song, S. Keller, U. K. Mishra, and S. P. DenBaars, Appl. Phys. Lett. **73**, 1370 (1998).

[35]P. G. Eliseev, P. Perlin, J. Lee, and M. Osinski, Appl. Phys. Lett. **71**, 569 (1997).

[36]S. W. Feng, Y. C. Cheng, Y. Y. Chung, C. C. Yang, K. J. Ma, C. C. Yan, C. Hsu, J. Y. Lin, and H. X. Jiang, Appl. Phys. Lett. **82**, 1377 (2003).

[37]M. A. Reshchikov and H. Morkoc, J. Appl. Phys. **97**, 061301 (2005).

[38]M. A. Reshchikov and R. Y. Korotkov, Phys. Rev. B **64**, 115205 (2001).

[39]M. Peter, A. Laubsch, W. Bergbauer, T. Meyer, M. Sabathil, J. Baur and B. Hahn, Phys. Status Solidi A **206**, 1125 (2009).

[40]M. A. Mastro, S. Maximenko, M. Gowda, B. S. Simpkins, P. E. Pehrsson, J. P. Long, A. J. Makinen, J. A. Freitas, J. K. Hite, C. R. Eddy, Jr., and J. Kim, J. Cryst. Growth **311**, 2982 (2009).

[41]Q. Li and G. T. Wang, Nano Lett. **10**, 1554 (2010); G. Wang, Q. Li, A.A. Talin, A. Armstrong, Y. Lin and J. Huang, ECS Trans. **19**(8), 55 (2009).

[42]X. Wang, X. Sun, M. Fairchild, and S. D. Hersee, Appl. Phys. Lett. **89**, 233115 (2006).

[43]A. Getty, E. Matioli, M. Iza, C. Weisbuch, and J. S. Speck, Appl. Phys. Lett. **94**, 181102 (2009).

[44]S. Saito, T. Narita, K. Zaima, K. Tachibana, H. Nago, G. Hatakoshi, and S. Nunoue, Phys. Status Solidi C **5**, 2195 (2008).

[45]J. A. Majewski and P. Vogl, MRS Internet J. Nitride Semicond. Res. **3**, 21 (1998).

[46]Z. Z. Bandić, T. C. McGill, and Z. Ikonic, Phys. Rev. B **56**, 3564 (1997).

[47]O. Ambacher, J. Phys. D: Appl. Phys. **31**, 2653 (1998).

[48]M. F. Ashby and L. M. Brown, Philos. Mag. **8**, 1083 (1963); **8**, 1649 (1963).

[49]K. Zang, Y. Wang, and S.J. Chua, Phys. Status Solidi C **6**, S514 (2009).